



# Directionally dependent strength and dilatancy behavior of soil–structure interfaces

Hans Henning Stutz<sup>1</sup> · Alejandro Martinez<sup>2</sup>

Received: 19 July 2020 / Accepted: 30 March 2021 / Published online: 28 April 2021  
© The Author(s), under exclusive licence to Springer-Verlag GmbH Germany, part of Springer Nature 2021

## Abstract

Soil–structure interfaces typically exhibit a shear behavior that is independent of the direction of relative displacement due to symmetry in the solid material’s surface profile. This experimental study investigates the interface shear behavior of surfaces with asymmetric profiles inspired by the scales of snake skin. The results of shear box interface tests on two sandy soils indicate that the peak and residual interface shear strengths and dilatancy are greater when the soil is displaced against the sharp edges of the asperities (cranial direction) than when the soil is displaced along the asperities (caudal direction). The experimental results indicate that the effect of asperity geometry on the interface shear response can be captured with the ratio of asperity length to asperity height ( $L/H$ ). Analysis of the stress–dilatancy behavior indicates that interfaces with a relatively short asperity length follow a classical flow rule developed for soils. However, the relationship between the mobilized stress ratio and the dilatancy rate is shown to be a function of the shearing direction and asperity geometry. Implementation of snake skin-inspired profiles on the surface of geotechnical structures may provide benefits in performance and efficiency during installation and service life. In general, the results of this study indicate the behavior of the soil–structure interfaces sheared in the cranial direction is similar to that of interfaces between soil and fully rough surfaces. In contrast, the behavior of the soil–structure interface sheared in the caudal direction shares characteristics with that of interfaces with smooth surfaces, including the mobilization of smaller a interface strength and dilation.

**Keywords** Deformation behavior · Roughness · Sand · Soil–structure interfaces · Surface anisotropy

## 1 Introduction

Understanding the interface shear and load transfer behavior between sandy soils and structural materials is essential for the design and performance of a variety of geotechnical structures such as axially loaded deep foundations, tunnel liners, and reinforced soil slopes. The transfer of load at soil–structure interfaces is governed by the structure’s surface properties and the properties and state of a thin layer of soil surrounding the structure. Recent research has explored the behavior of surfaces with

asymmetric surface profiles which mobilize different friction coefficients depending on the shearing direction [17, 18, 30]. These surfaces have the potential to lead to new design opportunities for the installation and performance of geotechnical engineering structures. For instance, O’Hara and Martinez [25] provide and Martinez and O’Hara [20] data from centrifuge pile load tests indicating that the skin friction of a pile with an asymmetric surface is significantly higher during tensile pullout than during jacking installation.

The effect of factors such as the soil density, particle shape, particle size, stress conditions, and loading path on the interface shear behavior with sandy soil has been quantified by various authors [3, 6, 14, 16, 22, 26, 27]. The surface properties of the structural material, such as the surface roughness and hardness, greatly impact the transfer of load across these interfaces [4, 35]. Particularly, the mobilized interface friction angle has a strong dependency on the surface roughness. For surfaces with a random

---

✉ Hans Henning Stutz  
hhs@cae.au.dk

<sup>1</sup> Department of Civil and Architectural Engineering, Aarhus University, Inge Lehmanns Gade 10, 8000 Aarhus C, Denmark

<sup>2</sup> Department of Civil and Environmental Engineering, University of California, Davis, California, USA

surface roughness form, the interface friction angle ( $\delta$ ) is smaller than or equal to the soil friction angle ( $\delta \leq \varphi$ ) [16]. For surfaces with a structured surface roughness form (e.g., ribbed surfaces), the apparent interface friction angle can be greater than the soil friction angle ( $\delta \leq \varphi$ ) due to the mobilization of passive resistances ahead of the protruding asperities [12, 16]. Soil–structure interfaces with surfaces with a low roughness are characterized by a slipping failure at the plane of contact between the surface and the soil, whereas soil–structure interfaces with surfaces with a large roughness are characterized by a failure within the contacting soil mass [9, 11, 12, 16, 35]. The surface roughness of the structural material is typically described using the maximum roughness ( $R_{\max}$ ), average roughness ( $R_a$ ), or normalized roughness ( $R_n$ ) parameters [8, 31, 35], which combine aspects of the surface’s asperity height and spacing as well as the mean particle size of the soil.

Research in bio-inspired geotechnics has recently gained increasing attention, with advances in soil–structure interaction, soil penetration and excavation, load transfer, and mass and thermal transport [15]. With regard to soil–structure interfaces, Martinez and Palumbo [17], Martinez et al. [18], and Stutz et al. [30] developed surfaces that can produce an interface shearing behavior that is dependent on the direction of relative displacement between the surface and the soil. These surfaces were bio-inspired from the asymmetric profile of ventral scales located along the underbelly of snakes. Martinez et al. [18] and Stutz et al. [30] showed that these surfaces mobilized greater peak and residual strength and dilation angles in the cranial direction (i.e., soil moving against the scales) than in the caudal direction (i.e., soil moving along the scales). This behavior is referred to here as “frictional directionality” or “frictional anisotropy.” In addition, O’Hara and Martinez [24, 25] showed that the snake skin-inspired surfaces also mobilized anisotropy during cyclic loading in terms of the mobilized interface friction angle and the degradation of shear strength. Martinez et al. [18] quantified the local soil deformations around asperities and concluded that cranial shearing induces larger local shear and volumetric strains than caudal shearing. This dependence of the interface shear behavior on the shearing direction is distinctly different from the effect of inherent soil fabric anisotropy [6, 33, 36–38].

Frictional directionality exists in many biological organisms (e.g., shark and snake skin, ant and spider legs) due to the asymmetric arrangement of nano- and micro-structural surface features [7, 23, 34]. The dependence of frictional interactions with the direction of relative movement usually serves the purpose of generating motion in a preferred direction [10, 13, 21]. Therefore, asymmetry in the surface profile appears to be an efficient method to create a bias in the transfer of load at soil–structure

interfaces. This paper presents the results of a series of interface shear tests between sandy soils and snake skin-inspired, asymmetric surfaces that examine the effects of sand density, particle shape, shearing direction, and asperity geometry on the interface shear strength and dilatancy behavior.

## 2 Materials and methods

### 2.1 Interface shear tests

Experiments were conducted in a direct interface shear test device [29] (Fig. 1). The soil specimen was contained within a shear box (No. 2 in Fig. 1) with a length of 100.0 mm, height of 32.5 mm, and width of 63.9 mm. Tests were conducted with constant normal load (CNL) boundary conditions at an applied normal stress of 75 kPa, unless otherwise noted. The horizontal and vertical forces were measured using a 5 kN load cell (ME—Messsystem, KD80s) and the vertical and horizontal deformations were measured using linear potentiometers (ME—Messsystem, LRW2-F-X-100). All tests were performed at a shearing rate of 1 mm/min consistent with previous sand–structure interface shear studies [18, 25]. All tests consisted of a single two-way cycle with a displacement amplitude of 10.5 mm such that the testing surface was displaced in the forward and backward direction in every test. This allows performing the test on the snake skin-inspired surfaces in two sequences: (1) cranial shearing during the first half cycle and caudal shearing during the second half cycle (referred to as a cranial-caudal test) and (2) caudal shearing during the first half cycle and cranial shearing during the

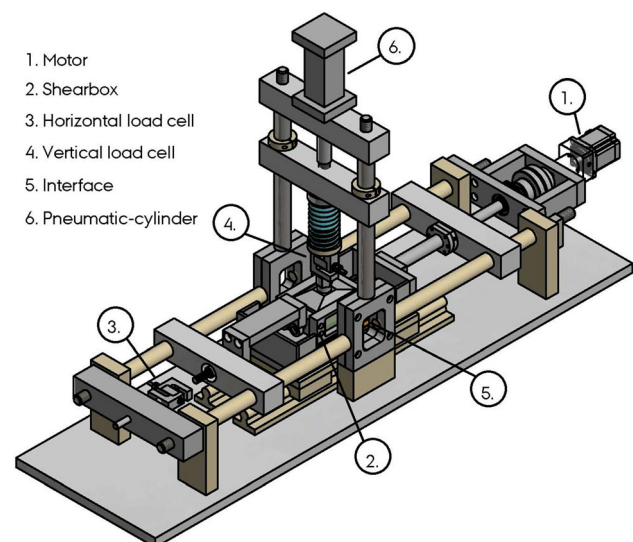


Fig. 1 Interface shear box device (after Stutz et al. [32])

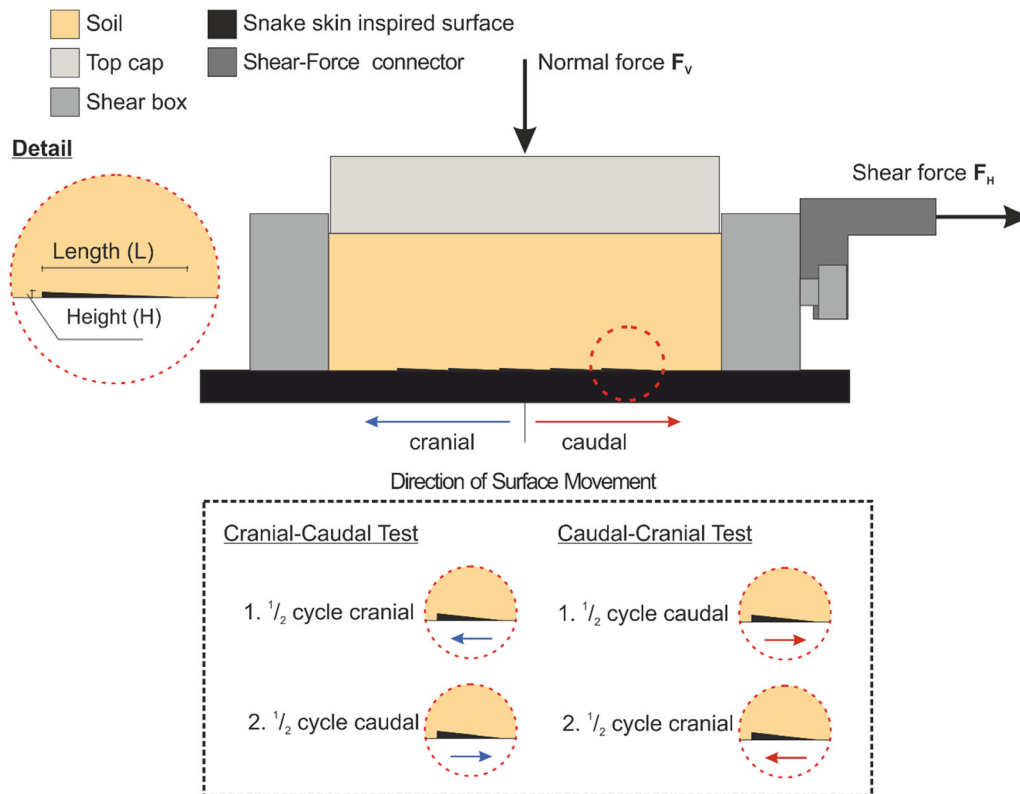


Fig. 2 Schematic of the interface shear testing configuration

second half cycle (referred to as a caudal-cranial test). Figure 2 presents a schematic of the shear box configuration.

### 2.2 Structural surfaces

Three surface types were used in this study: (1) six 3D printed snake skin-inspired surfaces, (2) one glued Ottawa 20–30 sand on steel surface, and (3) one 3D printed untextured surface. All surfaces had a central textured

section with a length of 80 mm and untextured sections at both ends with a length of 10 mm, as employed by other studies [3, 18, 19]. The untextured sections minimize the boundary effects caused by the shear box’s rigid sidewall. Table 1 provides a summary of the profile properties of all the surfaces used in this study.

The snake skin-inspired surfaces were 3D printed using stereolithography using a Form2 printer (Formlabs, Massachusetts). All the 3D printed surfaces were manufactured with Gray Pro photosensitive resin (Formlabs,

Table 1 Geometrical properties of the 3D printed snake skin-inspired surfaces

Surface ID	Scale height, $H$ (mm)	Scale length, $L$ (mm)	Length to height ratio, $L/H$
H03L13	0.3	13.0	43.3
H03L25	0.3	25.0	83.3
H03L36	0.3	36.0	120.0
H05L21	0.5	21.0	42.0
H05L41	0.5	41.0	82.0
H05L60	0.5	60.0	120.0
Rough	Glued Ottawa 20–30 Sand (Maximum surface roughness, $R_{max}$ ( $\mu\text{m}$ ) = 127.0)		
Untextured	Untextured (Maximum surface roughness, $R_{max}$ ( $\mu\text{m}$ ) = 1.54)		

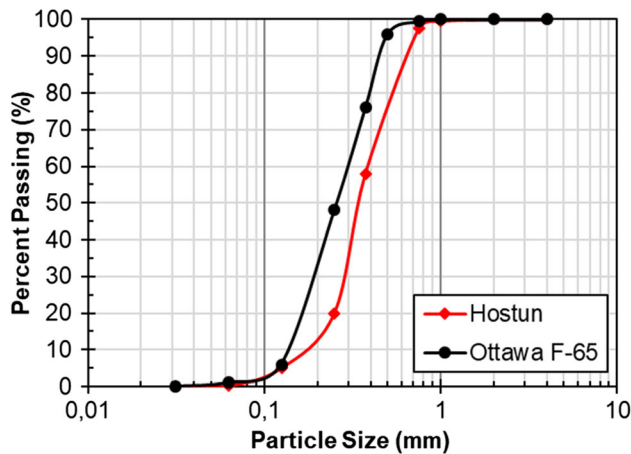


**Fig. 3** Grain size distribution of Hostun and Ottawa F-65 sands

Massachusetts), which has an ultimate tensile strength of 61 MPa, Young's modulus of 3.6 GPa, and Rockwell Hardness  $H$  of 45.7 [17]. The deposition layer thickness was 25  $\mu\text{m}$  to ensure a smooth surface finish. Testing by Martinez and Palumbo [17] confirmed that the 3D printed surfaces did not suffer significant wear during interface shear testing on the sand at normal stresses smaller than 400 kPa. The snake skin-inspired surfaces have different asperity heights ( $H$ ) and lengths ( $L$ ) (defined in Fig. 3):  $H$  was either 0.3 or 0.5 mm and  $L$  ranged from 13 to 60 mm. The height and length of the asperity were chosen to prevent large scale effects in the shear box. In addition, the asperity geometry was chosen based on previous studies that used snake skin-inspired surfaces [17, 18, 25, 30]. The combination of  $H$  and  $L$  values was selected such that the length to height ratio ( $L/H$ ) was similar between the surfaces with an asperity height of 0.3 and 0.5 mm (Table 1). The surface ID specifies the asperity height and length; for example, the H03L13 surface has an  $H$  of 0.3 mm and an  $L$  of 13 mm. Each test was performed in the cranial-caudal or caudal-cranial sequence depending on the orientation of the snake skin-inspired surface on the mounting plate.

The glued sand on steel surface has the highest surface roughness of all the surfaces ( $R_{\text{max}} = 127 \mu\text{m}$ , Table 1), which provided a baseline "fully rough" interface response. The untextured surface has the smallest surface roughness ( $R_{\text{max}} = 1.54 \mu\text{m}$ , Table 1), which provided a baseline "smooth" interface response.

### 2.3 Sand

This study used two well-characterized sands: Hostun and Ottawa F-65. Both are poorly graded quartz sands with slightly different mean particle sizes and different particle shape. Hostun sand is composed of angular grains [28],

**Table 2** Index and strength properties of Hostun sand and Ottawa F-65 sands

Parameter	Hostun Sand	Ottawa F-65
$G_s$	2.67	2.65
$D_{50}$ (mm)	0.35	0.20
$C_u$	1.72	1.61
$C_c$	1.05	0.96
$e_{\text{min}}^1$	0.65	0.51
$e_{\text{max}}^2$	1.00	0.83
$\phi_{\text{residual}}^3$ ( $^\circ$ )	39.0	30.0

<sup>1</sup>ASTM D 4253 - 00, <sup>2</sup>ASTM 4254 - 00, <sup>3</sup>from direct shear tests

whereas Ottawa F-65 sand is composed of rounded grains [2]. Table 2 presents the index and strength properties of the sands; Fig. 3 shows their grain size distribution. Two different relative densities ( $D_R$ ) were tested for each sand: 80% for dense and 50% for loose specimens. The specimens were prepared via air pluviation from a fixed height using a 3D printed pluviator. The  $D_R$  was controlled by modifying the flow rate of the sand exiting the pluviator.

### 3 Interface stress deformation behavior

A total of 52 interface shear tests were conducted on dense and loose Hostun and Ottawa F-65 sand specimens against the two reference surfaces and the six snake skin-inspired surfaces. This section provides the results of the tests performed against the reference surfaces as well as against the bio-inspired surfaces with an asperity height of 0.3 mm. The results for tests with the surface with an  $H$  of 0.5 mm are not included in this section for brevity.

The tests on the snake skin-inspired surfaces show a clear dependence of the mobilized shear stresses and dilatancy on the direction of movement. Figure 4 presents the shear stress-horizontal displacement and vertical displacement-horizontal displacement results for all tests on dense Hostun sand. The cranial-caudal test against surface H03L13 shows a response during the cranial-first direction that is similar to that of the test against the glued sand surface, with similar peak and residual shear stresses and maximum rate of dilation (Fig. 4a). During the caudal-second direction, the shear resistances take values that are intermediate between the untextured and the glued sand surfaces, and the volumetric response shows initial contraction. The caudal-cranial test indicates similar trends, where the caudal-first direction mobilized shear stresses that are slightly larger than those mobilized by the untextured surface and smaller than those mobilized by the cranial-first direction and glued sand tests (Fig. 4a). The

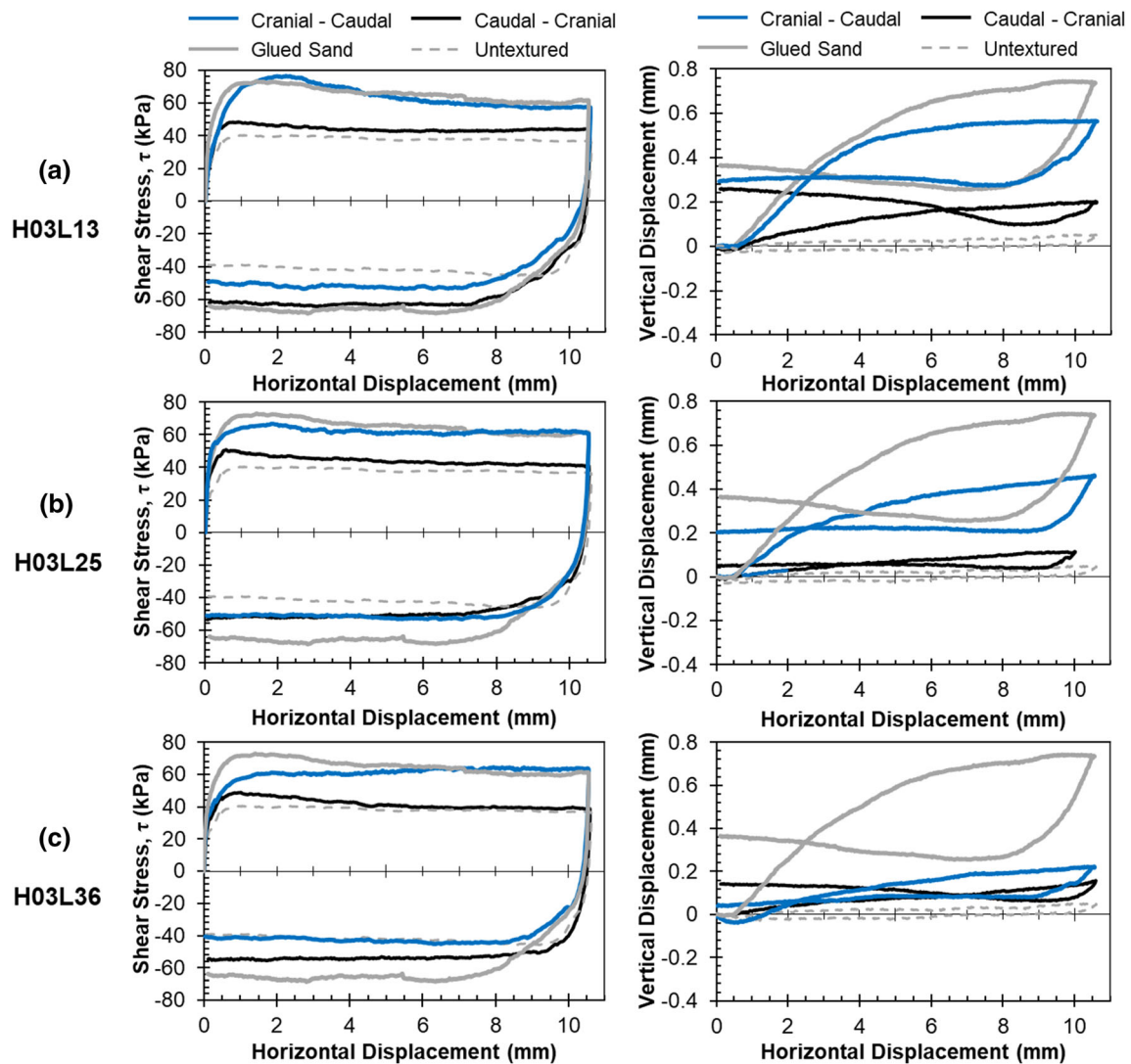


**Fig. 4** Shear stress and vertical displacement results of interface shear tests performed on dense ( $D_R = 80\%$ ) Hostun sand specimens against surfaces **a** H03L13, **b** H03L25, and **c** H03L36 ( $\sigma_n = 75$  kPa)

mobilized shear stresses for the cranial-second direction and the glued sand test have a similar magnitude.

The tests on the snake skin-inspired surfaces with greater asperity length indicate some similarities in behavior. Displacing these surfaces in the cranial direction resulted in larger shear resistances and dilatancy than displacing these surfaces in the caudal direction (Fig. 4b, c). The results show some differences as the asperity length is increased, such as the transition from a strain-softening shape of the cranial-first shear stress-horizontal displacement curve with an  $L$  of 13 mm to a strain hardening shape with an  $L$  of 36 mm (Fig. 4a, c). At large displacements, the shear stresses mobilized in the cranial-first direction by the three surfaces with different  $L$  converge to those mobilized by the glued sand surface. As  $L$  was increased, the shear resistances mobilized during the caudal-first and

caudal-second directions appear to converge to those mobilized by the untextured surface. In addition, while all the tests showed dilative tendencies due to the high  $D_R$  of the sand specimens, the rate of dilation and magnitude of total vertical displacement decreased as  $L$  was increased (Fig. 4a–c). It should be noted that the number of surface asperities decreases as  $L$  is increased: the H03L13 surface has six asperities, H03L21 has four asperities, and H03L36 has two asperities.

The results of the tests on dense Ottawa F-65 sand ( $D_R = 80\%$ ) specimens show similar trends as the tests on dense Hostun sand specimens (Fig. 5a–c). Cranial shearing mobilized larger shear stresses and dilative tendencies than caudal shearing, regardless of the testing sequence. The change in response as  $L$  was increased is also similar to that observed during the tests on Hostun sand. Owing to the

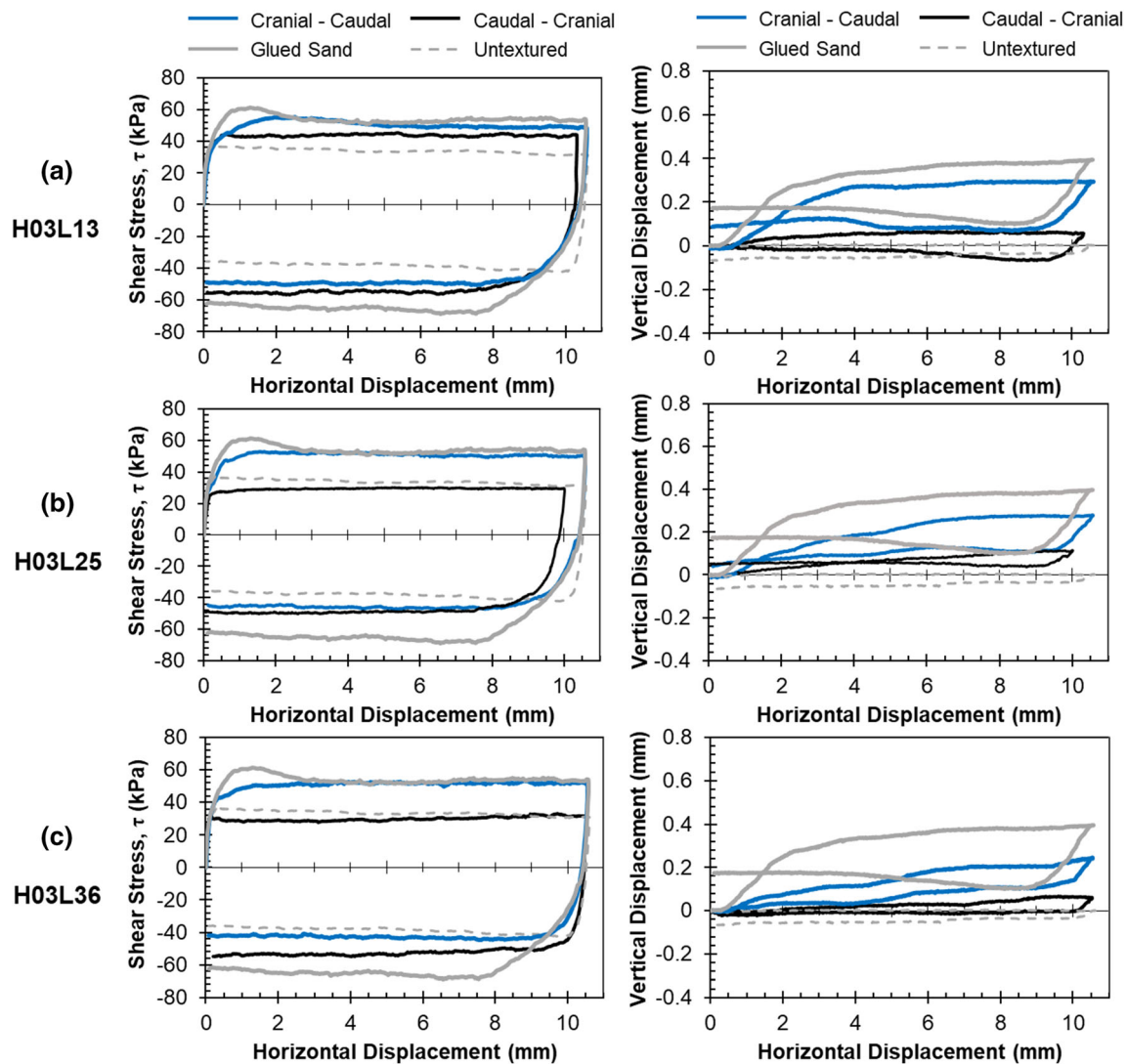


**Fig. 5** Shear stress and vertical displacement results of interface shear tests performed on dense ( $D_R = 80\%$ ) Ottawa F-65 sand specimens against surfaces **a** H03L13, **b** H03L25, and **c** H03L36 ( $\sigma_n = 75$  kPa)

more rounded shape of the Ottawa F-65 particles, the mobilized shear stresses and dilative vertical displacements were smaller as compared to the tests on Hostun sand.

Two additional test series were performed on loose specimens ( $D_R = 50\%$ ) of Hostun and Ottawa F-65 sand. The results on Hostun sand highlight similar trends as those shown by the tests on dense sand specimens. Larger shear resistances and dilatancy were mobilized during cranial shearing (during both cranial-caudal and caudal-cranial test sequences), and the dilative tendencies decreased as  $L$  was increased (Fig. 6a–c). The main differences between the tests on both types of loose and dense sand are the larger shear displacement required to mobilize stable residual shear stress and the smaller amount of dilation shown by the tests on loose sand. The tests on loose Ottawa F-65 specimens do not show a clear difference in the shear stresses and vertical displacements mobilized in the cranial

and caudal directions (Fig. 7a–c). In addition, the shear stresses and dilative vertical displacements mobilized during both the cranial-first and caudal-first directions were consistently lower than those mobilized by the glued sand surface.

Figure 8a–b presents results of cranial-first and caudal-first tests on dense Hostun sand against surface L13H03 at three different normal stress levels (75, 125, and 200 kPa). The results indicate that cranial shearing, mobilized greater shear resistances than caudal shearing. This can be observed by comparing the shear stresses during the first phase of shearing between the cranial first and caudal first tests as well as the shear stresses between the two different phases of a single test (i.e., cranial-first versus caudal-second in Fig. 8a and caudal-first versus cranial-second in Fig. 8b). These results are in agreement with the results presented in Figs. 4, 5, 6 and 7.

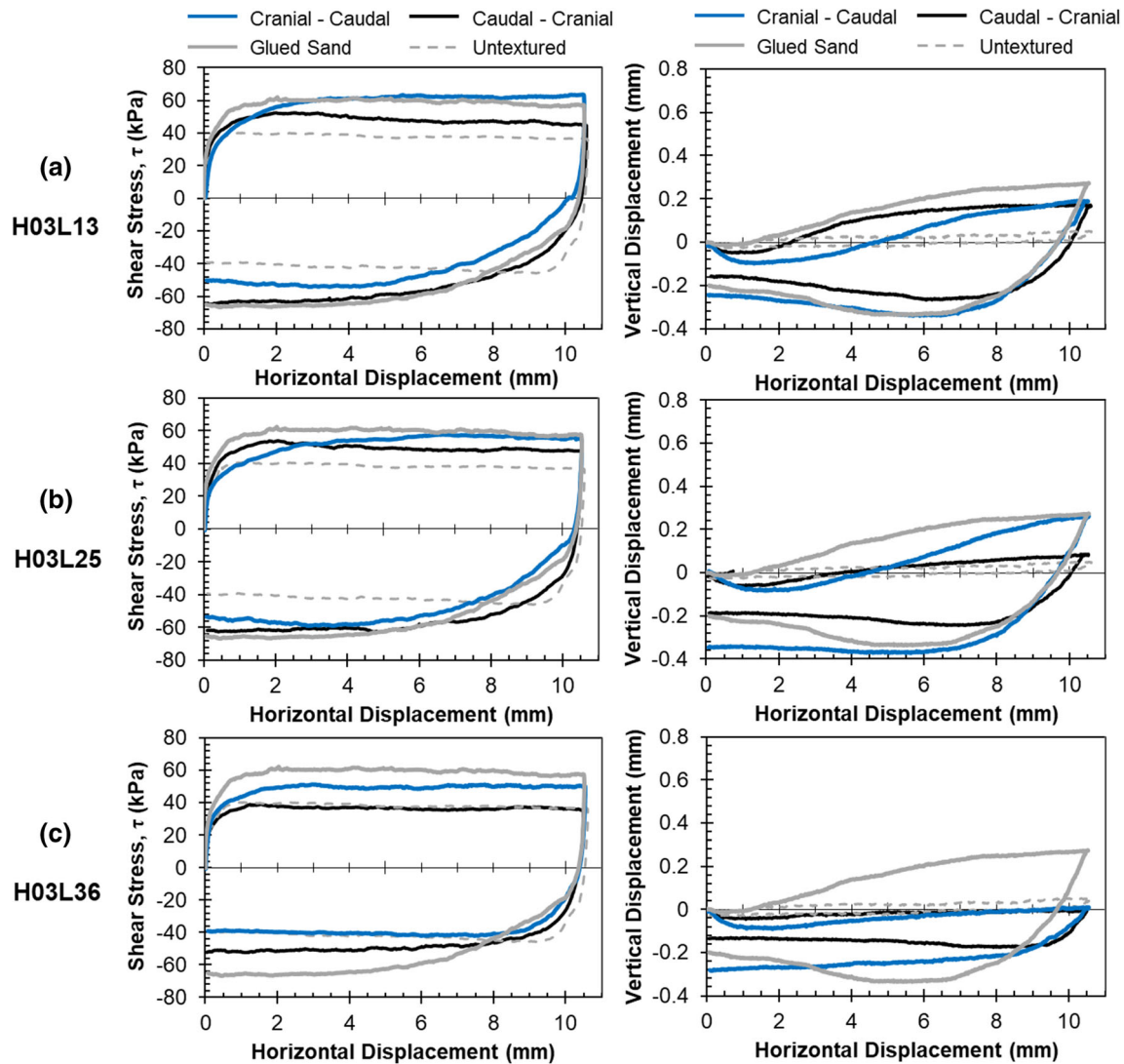


**Fig. 6** Shear stress and vertical displacement results of interface shear tests performed on loose ( $D_R = 50\%$ ) Hostun sand specimens against surfaces **a** H03L13, **b** H03L25, and **c** H03L36 ( $\sigma_n = 75$  kPa)

#### 4 Effect of asperity geometry and frictional directionality

Martinez et al. [18] postulated that the effect of the asperity length ( $L$ ) and height ( $H$ ) on the shear behavior of interfaces with snake skin-inspired surfaces could be described as a function of the ratio of the asperity length to height ( $L/H$ ). The authors provided results showing that roughness parameters such as the average ( $R_a$ ) and normalized roughness ( $R_n$ ) are not strongly correlated to the peak and residual shear resistances and maximum dilation angles mobilized by snake skin-inspired surfaces. Thus, the  $L/H$  ratio is adopted throughout this study to describe the experimental trends. The authors showed that the relationship between peak shear strength, residual shear strength, and dilation angle was better captured by  $L$

$H$  than by other surface roughness parameters, such as  $R_{max}$  and  $R_a$ . This is further explored here by comparing the results of tests with similar  $L/H$  values.

Figure 9a, b present peak and residual shear stresses and dilation angles obtained from the first half-cycle (i.e., cranial-first and caudal-first) of interface shear tests on Hostun sand as a function of the  $L/H$  ratio. The data clearly highlights the fact that greater peak and residual shear stresses and dilation angles were mobilized during cranial-first shearing than during caudal-first shearing. The figures also include data obtained from the glued sand and the untextured surfaces for reference. As shown, the cranial-first tests mobilized shear stresses and dilation angles that were close in magnitude to those mobilized by the glued sand surface. However, some of the data shows a decrease in shear stresses and dilation angle as the  $L/H$  ratio is

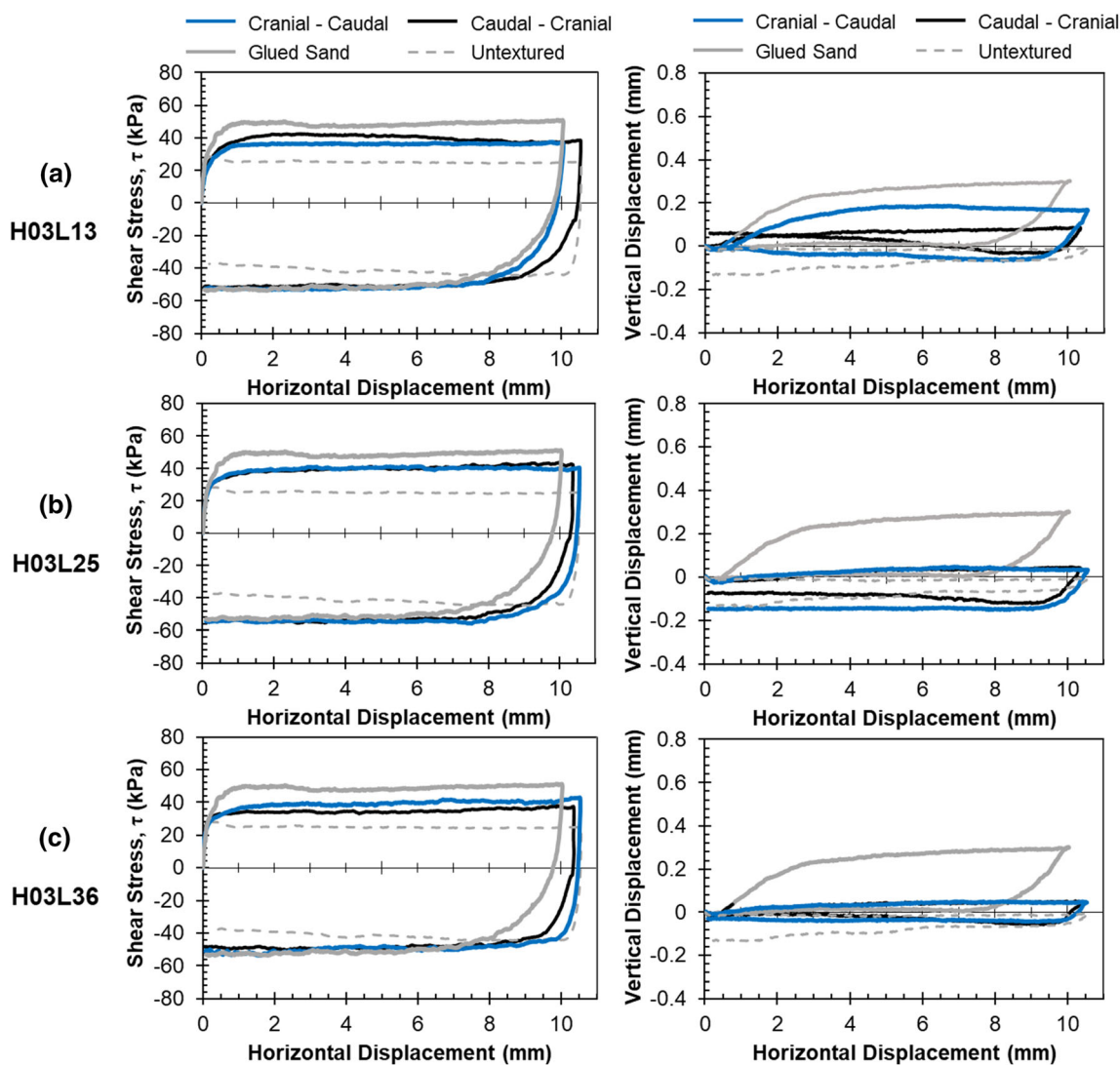


**Fig. 7** Shear stress and vertical displacement results of interface shear tests performed on loose ( $D_R = 50\%$ ) Ottawa F-65 sand specimens against surfaces **a** H03L13, **b** H03L25, and **c** H03L36 ( $\sigma_n = 75$  kPa)

increased, which is particularly visible for the peak shear stress and dilation angle of both dense and loose sand, while the residual stress for the dense sand showed no clear effect of changes in  $L/H$ . The caudal-first tests mobilized peak and residual shear stresses that were closer in magnitude to those mobilized by the untextured surface, and changes in  $L/H$  led to small or negligible changes.

The frictional anisotropy between the cranial and caudal directions in a single test (i.e. cranial-first versus caudal-second or caudal-first versus cranial-second) can be determined by comparing the shear stresses mobilized during the first and second directions. For reference, Fig. 2 presents an illustration of the sequence of cranial-first and caudal-first tests. This difference can be quantified with the Directional Frictional Resistance (DFR) parameter introduced by O'Hara and Martinez [25] and defined as follows:

$$\text{Directional Frictional Resistance, DFR} = \frac{|\tau_{\text{cranial}}|}{|\tau_{\text{caudal}}|} - 1 \quad (1)$$

where  $\tau_{\text{cranial}}$  and  $\tau_{\text{caudal}}$  are the shear stresses mobilized in a given test in the cranial and caudal directions, respectively. This parameter is defined such that a positive value indicates a greater shear resistance mobilized in the cranial direction, a value of zero indicates the same resistance mobilized in the cranial and caudal directions, and a negative value indicates a greater shear resistance mobilized in the caudal direction. The DFR parameter also normalizes the magnitude of the shear resistances to account, at least partially, for the influence of the normal effective stress magnitude and the sand's internal friction angle.

The DFR values calculated from the residual shear stresses have a dependency on the sand type, testing

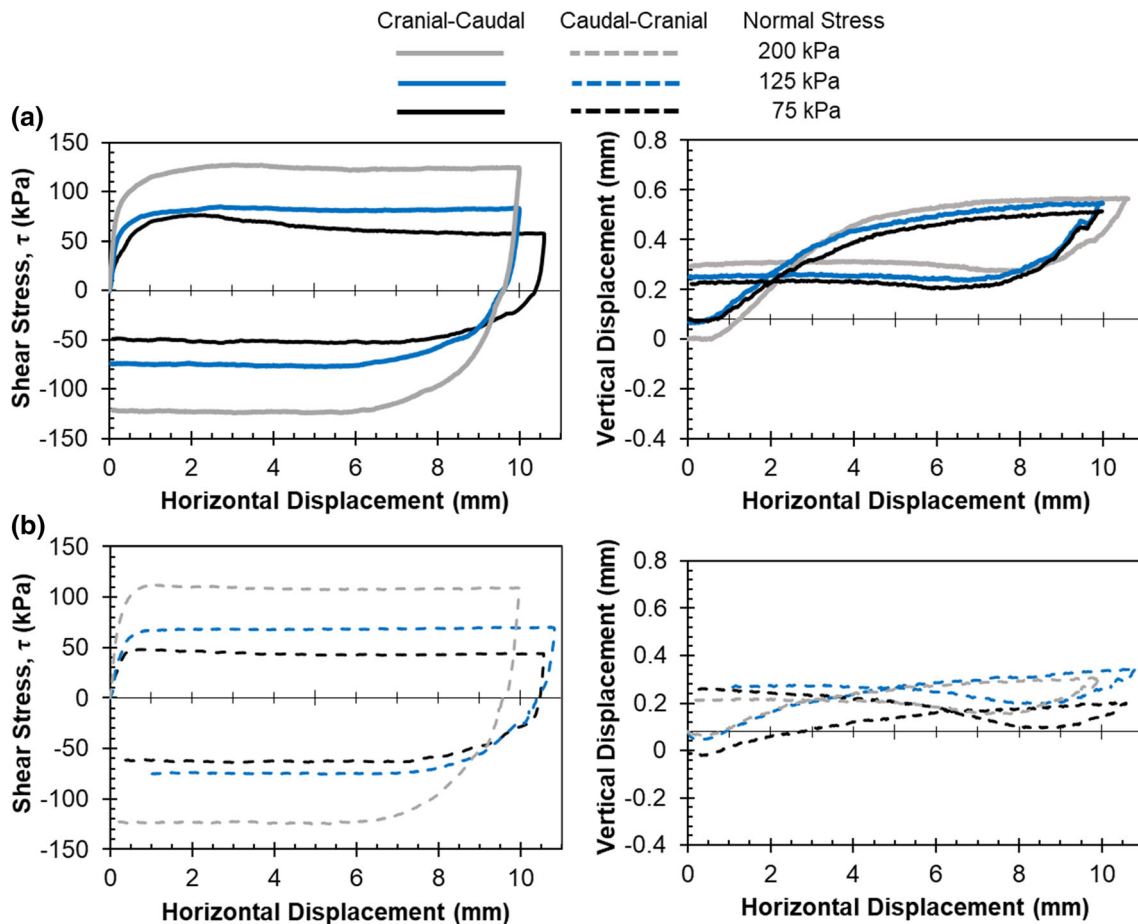


**Fig. 8** Shear stress and vertical displacement results of interface shear tests performed on dense ( $D_R = 80\%$ ) Hostun sand specimens against surfaces H03L13 at normal stresses of 75, 125, and 200 kPa: **a** Cranial-caudal tests and **b** caudal-cranial tests

sequence, and sand density. Average residual DFR values, calculated from the tests against all six snake skin-inspired surfaces, are shown in Fig. 10a, b, where the error bars indicate the data standard deviation. The caudal-first tests generally yielded larger DFR values, especially for the tests on Ottawa F-65 sand. The tests on loose specimens generally have a smaller, or even negative, DFR value. In the case of cranial-first tests on loose Ottawa F-65 sand, the negative DFR value indicates that larger shear resistances were mobilized during the caudal-second direction. These results indicate that the testing sequence influences the difference in shear resistances mobilized during cranial and caudal shearing. The results reported here are in agreement with those presented by O'Hara and Martinez [24] from cyclic constant normal stiffness (CNS) interface shear tests. The authors' results indicate that the DFR values are generally greater for caudal-first tests than for cranial-first tests and that negative DFR values can be mobilized during the latter testing sequence. While the dependence of DFR on the testing sequence needs to be further investigated, the results from O'Hara and Martinez [24] as well as those

from this investigation suggest that negative DFR values tend to be mobilized in cranial-first tests with conditions associated with more pronounced sand contractive behavior, such as specimens with smaller  $D_R$  and sands with less pronounced dilative tendencies (i.e., more rounded grains).

Figure 10a, b also includes data from the tests on the glued sand and untextured surfaces. To include data from these tests, Eq. (1) was slightly modified by taking the shear stress mobilized in the first direction in the numerator and that mobilized in the second direction in the denominator. The results indicate that with this definition of DFR, all the tests on glued-sand and untextured surfaces yielded negative values with a small magnitude. This means that the shear resistances in the second direction were consistently somewhat greater than in the first direction. The reason for this trend may be a dependency of the interface strength on the stress history or on the evolution of the soil fabric or a slight bias in the experimental device. Nonetheless, the comparison of the DFR results from snake skin-inspired surfaces and glued sand and untextured surfaces indicates that significantly greater frictional

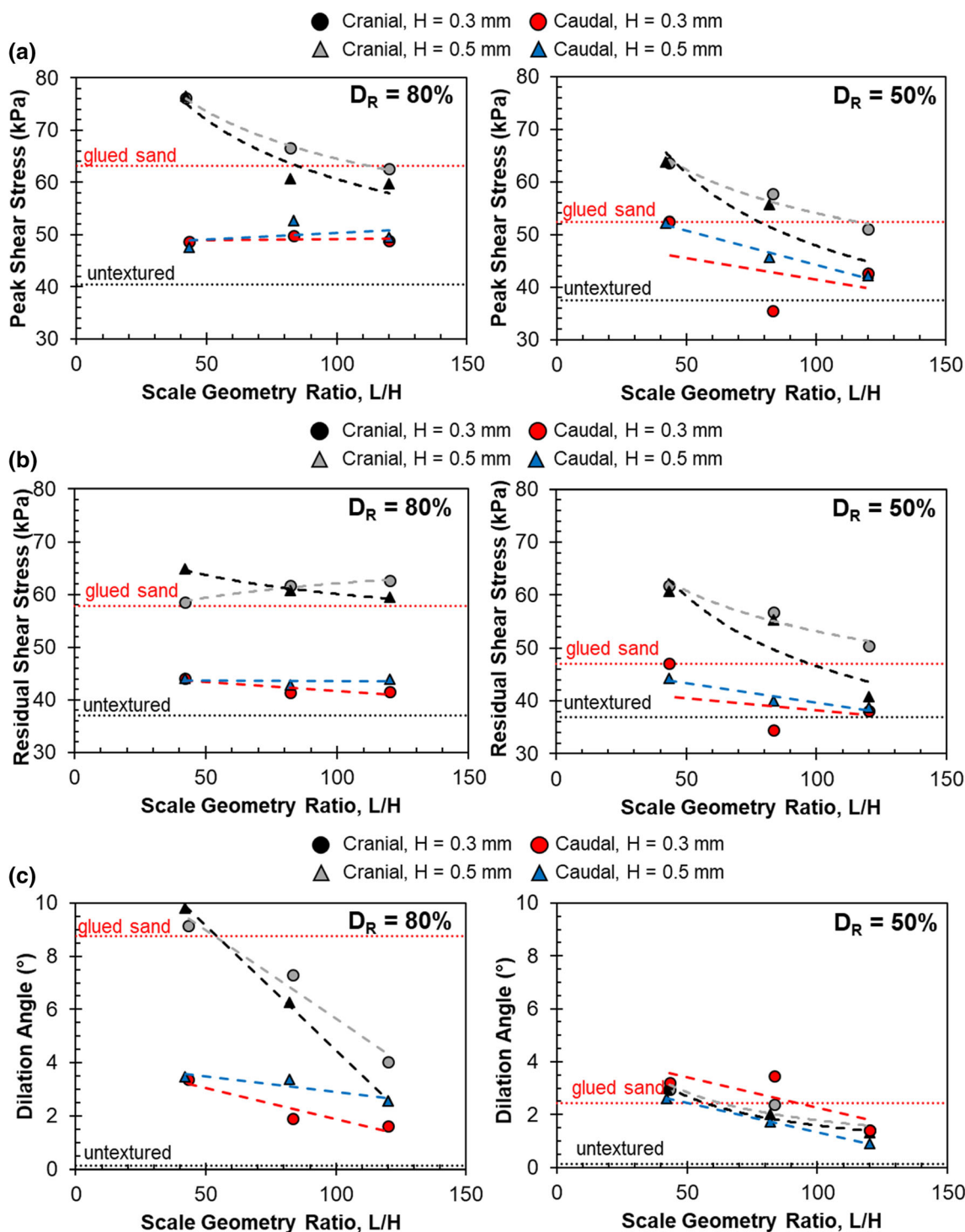


**Fig. 9** **a** Peak shear stress, **b** residual shear stress, and **c** dilation angle mobilized during cranial-first and caudal-first tests on Hostun sand at  $D_R$  of 80% and 50% ( $\sigma_n = 75$  kPa)

anisotropy can be mobilized by the bio-inspired surfaces, particularly for tests performed in the caudal-first, cranial-second sequence.

### 5 Stress-dilatancy response

Interfaces composed of sand and rough surfaces have been shown to exhibit a stress-dilatancy behavior similar to that of sand-on-sand shearing. Lings and Dietz [14], Dove and

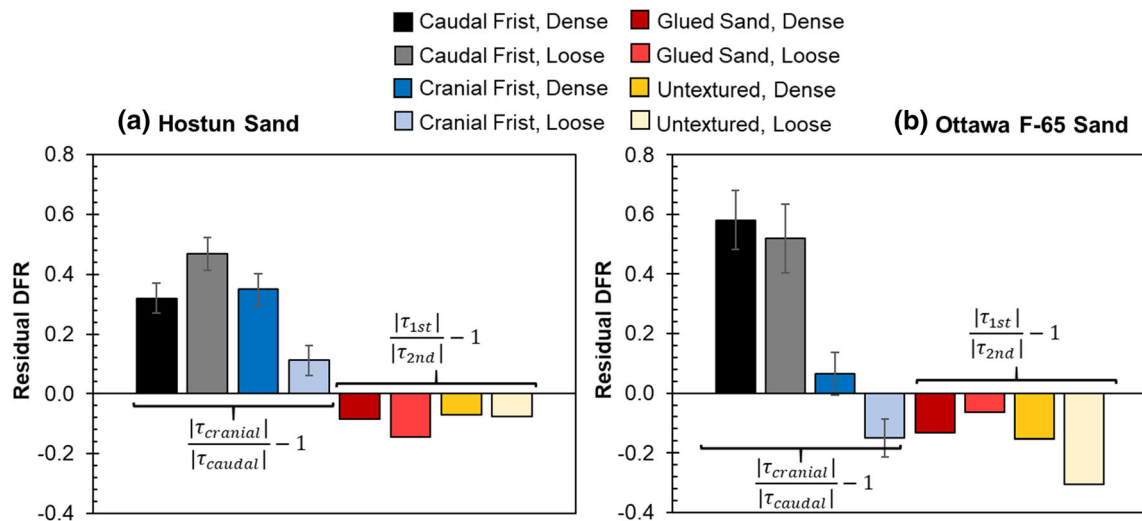


**Fig. 10** Average residual directional frictional resistance for tests with snake skin-inspired surfaces in the cranial-first and caudal-first sequence and for tests on glued sand and untextured surfaces. Tests on **a** Hostun and **b** Ottawa F-65 sand ( $\sigma_n = 75$  kPa) Note: the error bars show the standard deviation on cranial-first and caudal-first tests

Jarrett [5], and Afzali-Nejad et al. [1] have shown that this type of interface follows classical flow rules for sand-on-sand shearing. In particular, Lings and Dietz [14] showed that rough interfaces followed the Taylor [32] flow rule, which relates the mobilized stress ratio with the residual stress ratio and dilatancy rate as follows:

$$\left(\frac{\tau}{\sigma'_n}\right) = \left(\frac{\tau}{\sigma'_n}\right)_{\text{residual}} + \left(\frac{du_y}{du_x}\right) \quad (2)$$

where  $du_y$  is the vertical displacement increment and  $du_x$  is the horizontal displacement increment. It should be noted that this equation is only valid between the peak and residual shearing stages and that different studies have used different definitions for the residual state, often referring to it either as the steady-state or post-peak state.

Plotting the results of the interface shear tests in stress ratio-dilatancy rate space reveals the coupling between strength and dilatancy. Figure 11a, b shows the results of the tests on dense Hostun and Ottawa F-65 sand against the glued sand and untextured surfaces. The figures also include straight lines with a slope of unity fitted to the data with a positive dilatancy rate that represents the flow rule described by Eq. (2). The residual stress ratio takes values of 0.80 for the Hostun sand and 0.62 for the Ottawa F-65 sand. As shown, the data for the test against the glued sand surface follows the flow rule line reasonably well while the data for the test against the smoother untextured surface plots below the flow rule line, supporting the observations by Lings and Dietz [14].

The results of tests on dense Hostun and Ottawa F-65 sand specimens against the H03L13 surface indicate that the stress-dilatancy response during the cranial-first directions are described reasonably well by the flow rule line in

Eq. (2) (Fig. 11c, d). In addition, the cranial-first data plots similar to that of the test on the glued sand surface. These results agree with findings from Martinez et al. [18] who showed using particle image velocimetry (PIV) that shearing against surfaces with an  $L/H$  ratio of about 43 develops a uniform shear band where the sand deformations localize in a similar fashion as tests performed with glued sand surfaces. The stress-dilatancy response of the caudal-first tests is similar to that of the test on the untextured surface, in agreement with the shear stress and vertical displacement results presented in Figs. 4, 5, 6, 7. The results from tests on the H05L21 surfaces are presented in Fig. 11e, f. These results indicate a similar response as those on the H03L13 surface and support the observation that the  $L/H$  is an adequate parameter for capturing the strength and dilatancy behavior of snake skin-inspired surfaces.

The asperity geometry influences the interface shear behavior. Figure 12a–f presents the cranial-first and caudal-first data for tests on dense Hostun and Ottawa F-65 sand against surfaces H03L13 ( $L/H = 43.3$ ), H03L21 ( $L/H = 83.3$ ), and H03L36 ( $L/H = 120.0$ ), where the solid line represents the flow rule in Eq. (2). As previously shown, the H03L13 surface exhibited a cranial-first behavior similar to that of the test against the glued sand surface (Figs. 11c, d, 12a, b). The stress-dilatancy response is affected by the surface’s  $L/H$ , as observed in the cranial-first data. This is most apparent for tests against surfaces with an  $L/H$  of 120, indicating that the stress ratio and dilatancy rate follow a line with a negative slope, shown in Fig. 12e, f with a dashed line. This suggests a change in the load transfer mechanism from one described by the flow rule in Eq. (2) for the surface with an  $L/H$  of 43.3 to a

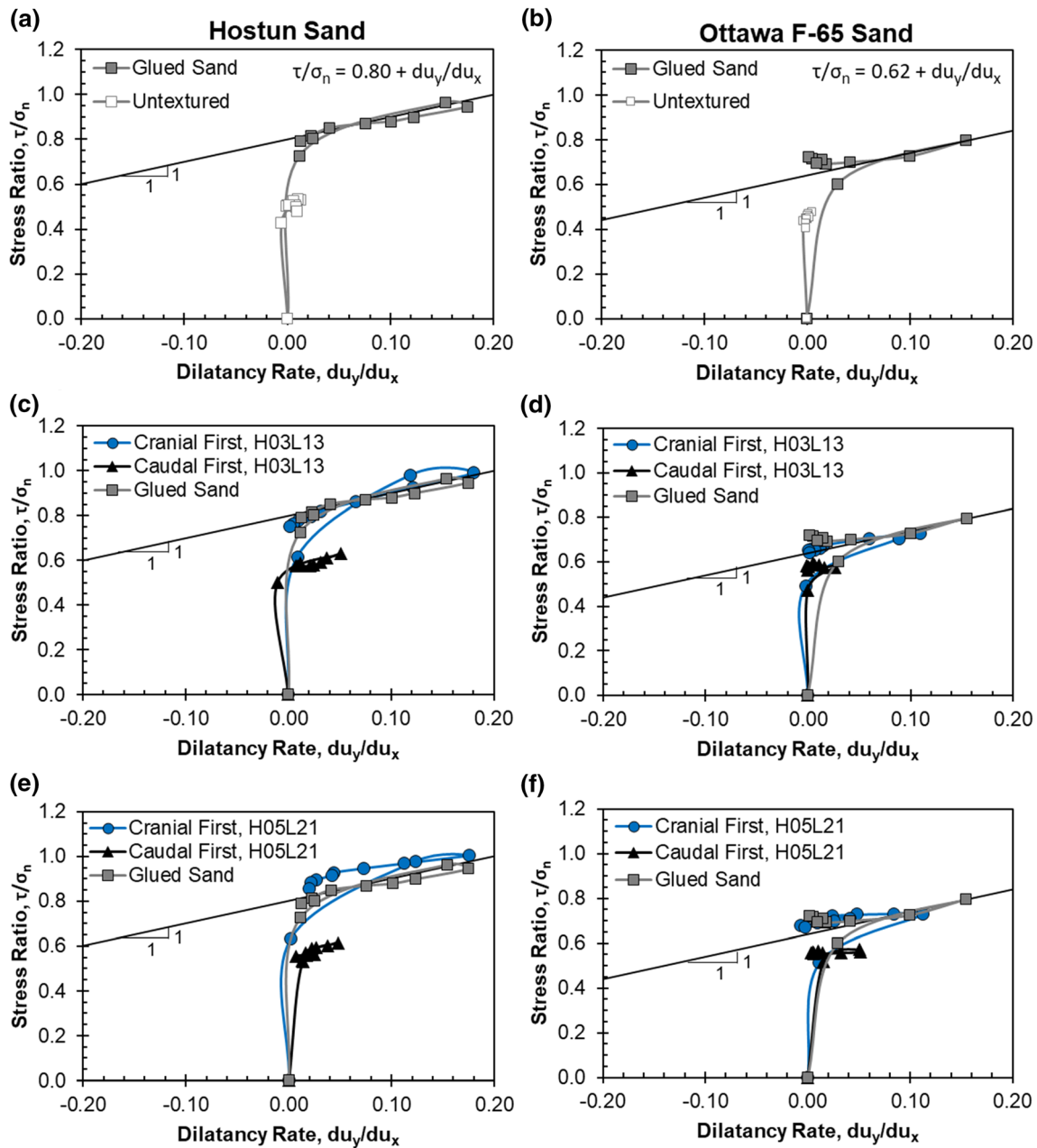


**Fig. 11** Stress-dilatancy relationship for the first direction of tests on Hostun sand against **a** glued sand and untextured, **c** H03L13, and **e** H05L21 surfaces and on Ottawa F-65 sand against **b** glued sand and untextured, **d** H03L13, and **f** H05L21 surfaces ( $D_R = 80\%$ ,  $\sigma_n = 75$  kPa)

mechanism where the stress ratio can increase while the dilatancy rate decreases for the surface with an  $L/H$  of 120. This observation supports the soil deformation measurements from PIV presented by Martinez et al. [2]. As indicated in Martinez et al. [2] the surfaces with an  $L/H$  greater than 80.0 create localized zones of soil deformation ahead of each asperity. The zones of localized soil deformation appear to not interact with each other, likely leading to load transfer in terms of passive conditions that subsequently lead to local increases in mean effective stress in the zone ahead of the asperities.

The testing sequence influences the shear resistances mobilized in the first and second directions (Fig. 10). This is further explored using the stress-dilatancy framework. Figure 13a, b presents the results of cranial-first and caudal-first tests, respectively, on dense Hostun sand against the H03L12 ( $L/H = 43.3$ ) surface. As shown, the cranial stress ratio-dilatancy rate data, whether in the first (Fig. 13a) or second direction (Fig. 13b), converges towards the flow rule line. The caudal-first and caudal-second data consistently plotted below the cranial data, in agreement with the smaller shear resistances and dilatancy

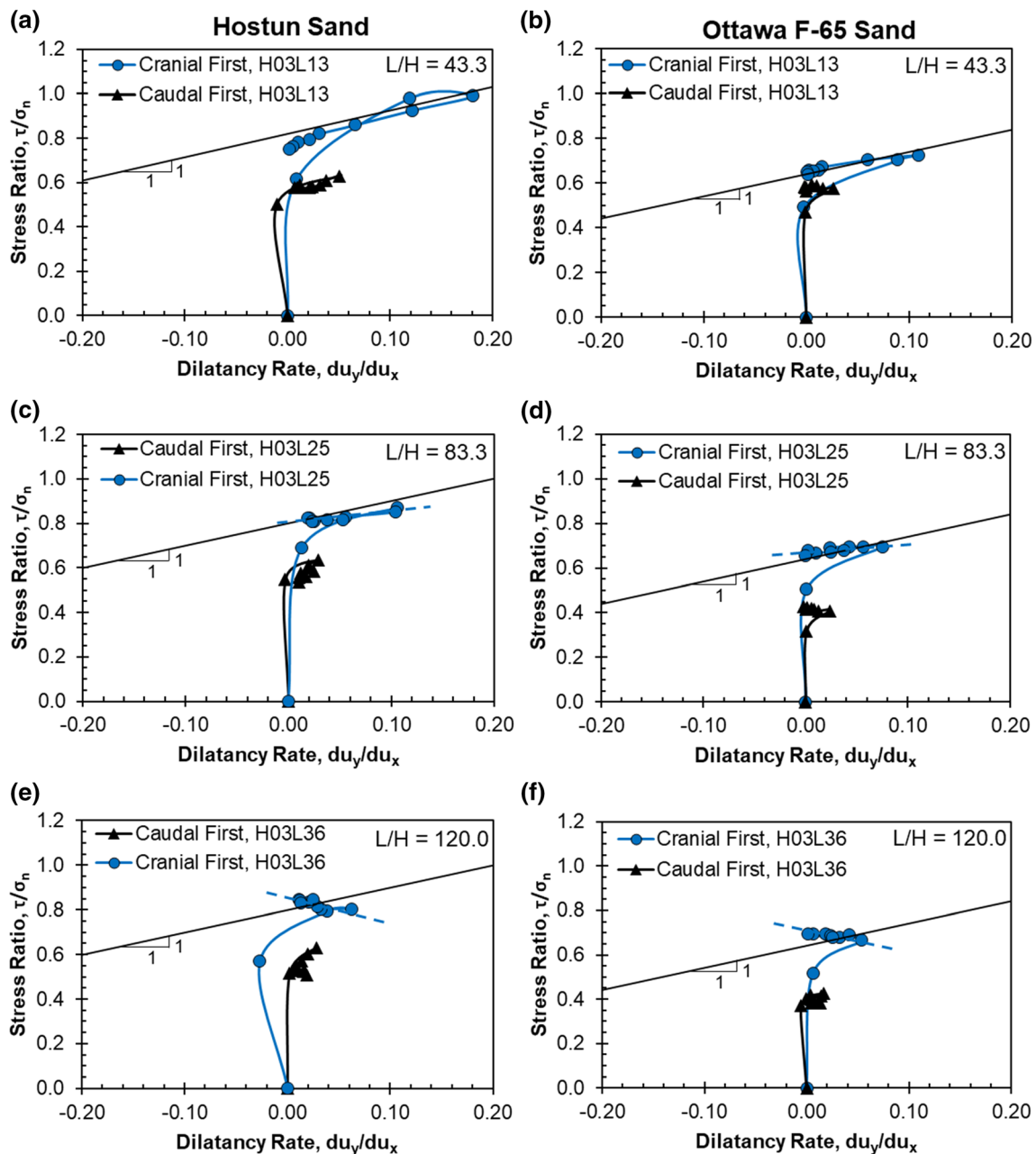


**Fig. 12** Stress-dilatancy relationship for the first direction of tests on Hostun and Ottawa F-65 sands against snake skin-inspired surfaces with  $L/H$  of **a** and **b** 43.3, **c** and **d** 83.3, and **e** and **f** 120.0 ( $D_R = 80\%$ ,  $\sigma_n = 75$  kPa)

reported in Figs. 4, 5, 6 and 7. The caudal shearing data exhibits a similar trend as the untextured surface data (Fig. 11), and its position with respect to the flow rule is in agreement with observations by Lings and Dietz [14] for surfaces with low surface roughness. The results from tests on dense Hostun sand against the H05L21 surface ( $L/H = 42$ ) exhibit the same trends as those described for the H03L13 surface (Fig. 13c, d).

## 6 Conclusions

The results presented in this paper highlight the ability of surfaces with asymmetric profiles to create a bias in the load transfer behavior of soil-structure interfaces. Tests were performed between two sands (i.e., Hostun and Ottawa F-65) and surfaces with asymmetric profiles inspired by the belly scales of snakes. The results indicate that shearing in the cranial direction (i.e., soil moving against the asperities) mobilized greater peak and residual

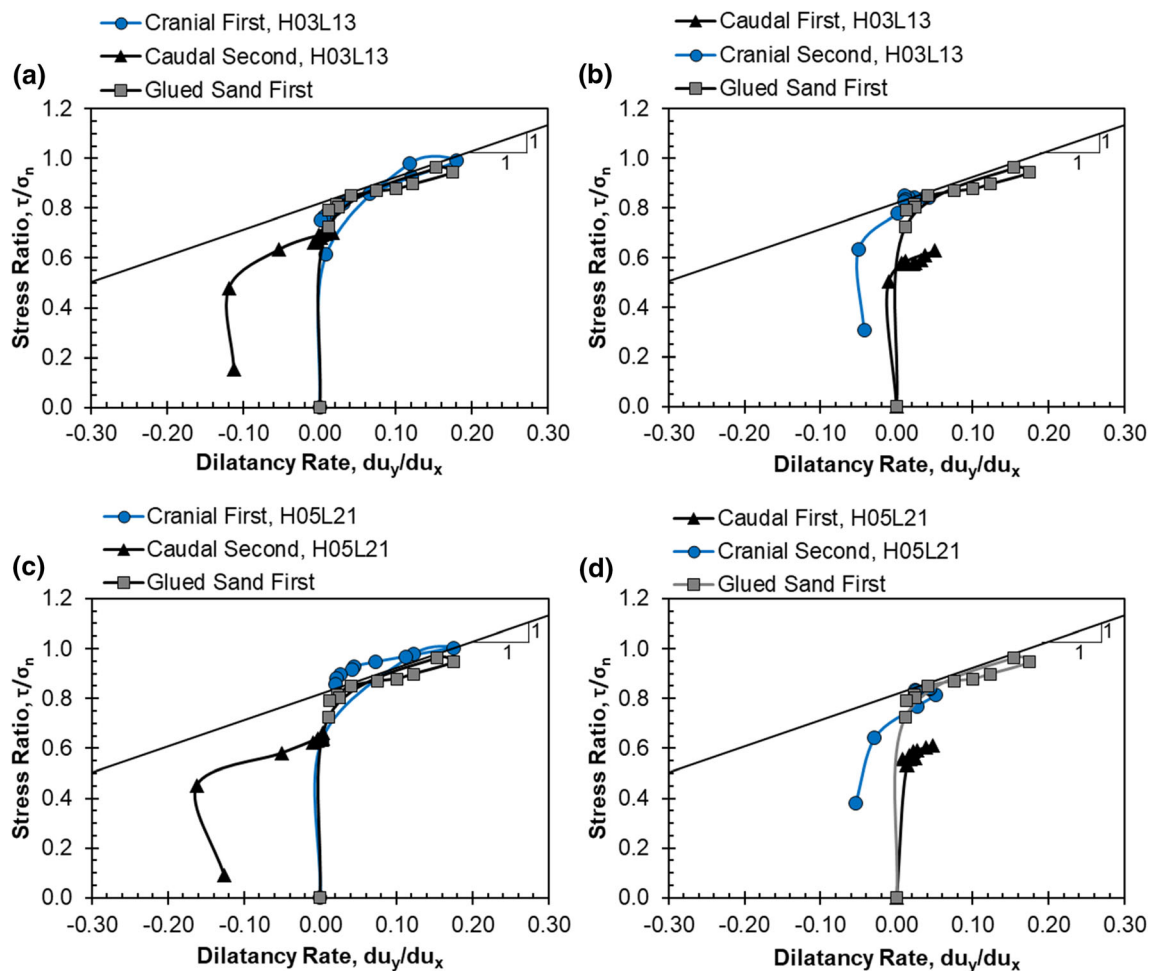


**Fig. 13** Stress-dilatancy relationship for the first and second directions of tests on Hostun sand. **a** Cranial-caudal and **b** caudal-cranial test against surface H03L13 and **c** cranial-caudal and **d** caudal-cranial test against surface H05L21 ( $D_R = 80\%$ ,  $\sigma_n = 75$  kPa)

shear resistances than shearing in the caudal direction (i.e. soil moving along the asperities). Also, the volumetric response was consistently more dilative during cranial shearing than during caudal shearing. These trends were verified for tests on dense and loose specimens of both sand types at different magnitudes of normal stress. The interface shear behavior in the cranial direction is similar to that of an interface with a fully rough surface, while the shear behavior in the caudal direction is similar to that of an interface with an untextured, smooth surface. The length and height of the asperities influence the mobilized shear resistances and volumetric changes, which can be reasonably captured by the asperity length to height ratio ( $L/H$ ). The difference in interface strength (i.e., frictional directionality) are shown to depend on the sand type, sand density, and testing sequence. The only case in which greater shear resistances were mobilized during caudal shearing is tests on loose Ottawa F-65 specimens, in agreement with previously published results. In addition, the results show that the shear-dilatancy behavior during

cranial shearing with a surface with small  $L/H$  ratio is successfully captured by the classical Taylor flow rule. In contrast, the shear-dilatancy behavior with surfaces with large  $L/H$  ratios deviates from the Taylor flow rule, suggesting that loads are increasingly being transferred by other mechanisms such as passive resistances.

Transfer of load between soils and structures that is directionally dependent could be beneficial for geotechnical applications. For example, many geotechnical structures are loaded in opposite directions during their installation and service life, such as piles, suction caissons and anchors for offshore structures. In such a situation, installation in the caudal direction could lead to a smaller skin friction than during subsequent tensile loading. Another example is deep foundations in settling ground, where installation in the cranial direction could decrease the magnitude of the negative skin friction generated above the neutral plane with respect to the positive skin friction mobilized below the neutral plane. Further research is required to evaluate the benefits of using asymmetric

surfaces on geotechnical structures. Particularly, centrifuge and full-scale field tests as well as numerical simulations could provide an evaluation of the behavior in light of installation effects and service life loading conditions.

**Acknowledgement** The assistance of Stanislav Gorb, Lars Heepe, and Halvor Tram Tramsen in manufacturing the surfaces and discussing frictional anisotropy is acknowledged. This material is based upon work supported in part by the Engineering Research Center Program of the National Science Foundation under NSF Cooperative Agreement No. EEC-1449501. Any opinions, findings, and conclusions or recommendations expressed in this material are those of the author(s) and do not necessarily reflect those of the National Science Foundation.

## References

- Afzali-Nejad A, Lashkari A, Tabatabaie Shourijeh P (2017) Influence of particle shape on the shear strength and dilation of sand-woven geotextile interfaces. *Geotext Geomem* 45(1):54–66. <https://doi.org/10.1016/j.geotextmem.2016.07.005>
- Carey TJ, Stone N, Kutter BL (2020) Grain Size Analysis and Maximum and Minimum Dry Density Testing of Ottawa F-65 Sand for LEAP-UCD-2017. In: Kutter B, Manzari M, Zeghal M (eds) *Model Tests and Numerical Simulations of Liquefaction and Lateral Spreading*. Springer, Cambridge
- DeJong JT, Westgate ZJ (2009) Role of initial state, material properties, and confinement condition on local and global soil-structure interface behavior. *J Geotech Geoenviron Eng* 135(11):1646–1660. [https://doi.org/10.1061/\(ASCE\)1090-0241\(2009\)135:11\(1646\)](https://doi.org/10.1061/(ASCE)1090-0241(2009)135:11(1646))
- Dove J, Frost JD (1999) Peak friction behavior of smooth geomembrane-particle interfaces. *J Geotech Geoenviron Eng* 125(7):544–555. [https://doi.org/10.1061/\(ASCE\)1090-0241\(1999\)125:7\(544\)](https://doi.org/10.1061/(ASCE)1090-0241(1999)125:7(544))
- Dove J, Jarrett J (2002) Behavior of dilative sand interfaces in a geotribology framework. *J Geotech Geoenviron Eng* 128(1):25–37. [https://doi.org/10.1061/\(ASCE\)1090-0241\(2002\)128:1\(25\)](https://doi.org/10.1061/(ASCE)1090-0241(2002)128:1(25))
- Farhadi B, Lashkari A (2017) Influence of soil inherent anisotropy on behavior of crushed sand-steel interfaces. *Soils Found* 57(1):111–125. <https://doi.org/10.1016/j.sandf.2017.01.008>
- Filippov A, Gorb SN (2013) Frictional-anisotropy based systems in biology: structural diversity and numerical model. *Sci Rep* 3:1240. <https://doi.org/10.1038/srep01240>
- Fioravante V, Ghionna VN, Pedroni S, Porcino D (1999) A constant normal stiffness direct shear box for soil-solid interface tests. *Rivista Italiana Di Geotecnica* 3:7–22
- Han F, Ganju E, Salgado R, Prezzi M (2018) Effects of Interface roughness, particle geometry, and gradation on the sand-steel interface friction angle. *J Geotech Geoenviron Eng* 144(12):1990. [https://doi.org/10.1061/\(ASCE\)GT.1943-5606.0001990](https://doi.org/10.1061/(ASCE)GT.1943-5606.0001990)
- Hazel J, Stone M, Grace MS, Tsukruk VV (1999) Nanoscale design of snake skin for reptation locomotions via friction anisotropy. *J Biomech* 32(5):477–484. [https://doi.org/10.1016/S0021-9290\(99\)00013-5](https://doi.org/10.1016/S0021-9290(99)00013-5)
- Hebeler GL, Martinez A, Frost JD (2015) Shear zone evolution of granular soils in contact with conventional and textured CPT friction sleeves. *KSCCE J Civil Eng* 1–167:1267. <https://doi.org/10.1007/s12205-015-0767-6>
- Irsyam M, Hryciw RD (1991) Friction and passive resistance in soil reinforced by plane ribbed inclusions. *Géotechnique* 41(4):485–498. <https://doi.org/10.1680/geot.1991.41.4.485>
- Klein MCG, Deuschle JK, Gorb SN (2010) Material properties of the skin of the Kenyan sand boa *Gongylophis colubrinus* (Squamata, Boidae). *J Comp Physiol A* 196:659–668. <https://doi.org/10.3762/bjnano.9.243>
- Lings ML, Dietz MS (2005) The peak strength of sand-steel interfaces and the role of dilation. *Soils Found* 45(6):1–14
- Martinez A, DeJong J, Akin I, Aleali A, Arson C, Atkinson J, Bandini P, Baser T, Borela R, Boulanger R, Burrall M, Chen Y, Collins C, Cortes D, Dai S, DeJong T, Del Dottore E, Dorgan K, Fragaszy R, Frost D, Full R, Ghayoomi M, Goldman D, Gravish N, Guzman IL, Hambleton J, Hawkes E, Helms M, Hu DL, Huang L, Huang S, Hunt C, Irschick D, Lin H, Lingwall B, Marr WA, Mazzolai B, McInroe B, Murthy T, O'Hara K, Porter M, Sadek S, Sanchez M, Santamarina C, Shao L, Sharp J, Stuart H, Stutz HH, Summers AP, Tao J, Tolley M, Treers L, Turnbull K, Valdes R, van Passen L, Viggiani G, Wilson D, Wu W, Yu X, Zheng J (2020) Bio-inspired geotechnical engineering: principles, current work, opportunities, and challenges. *Géotechnique* (accepted). <https://doi.org/10.1680/jgeot.20.P.170>
- Martinez A, Frost JD (2017) The influence of surface roughness form on the strength of sand-structure interfaces. *Geotechnique Letters* 7(1):104–111. <https://doi.org/10.1680/jgele.16.00169>
- Martinez A, Palumbo S (2018) Anisotropic shear behavior of soil-structure interfaces: bio-inspiration from snake skin. *Proceedings of ASCE IFCEE 2018 Conference Orlando, FL*
- Martinez A, Palumbo S, Todd BD (2019) Bio-Inspiration for anisotropic load transfer at soil-structure interfaces. *J Geotech Geoenviron Eng* 145(10). [https://doi.org/10.1061/\(ASCE\)GT.1943-5606.0002138](https://doi.org/10.1061/(ASCE)GT.1943-5606.0002138)
- Martinez A, Stutz HH (2019) Rate effects on the interface shear behaviour of normally and overconsolidated clay. *Géotechnique* 69(9):801–815. <https://doi.org/10.1680/jgeot.17.P.311>
- Martinez A, O'Hara KV (2020) Skin friction directionality in monotonically- and cyclically-loaded bio-inspired piles in sand. *DFI Journal* 14(3)
- Marvi H, Hu DL (2012) Friction enhancement in concertina locomotion of snakes. *J Royal Soc Interface* 9(76):3067–3080. <https://doi.org/10.1098/rsif.2012.0132>
- Mortara G, Mangiola A, Ghionna VN (2007) Cyclic shear stress degradation and post-cyclic behaviour from sand-steel interface direct shear tests. *J Can Geotech* 44(7):739–752. <https://doi.org/10.1139/t07-019>
- Motta P, Habegger ML, Lang A, Hueter R, Davis J (2012) Scale morphology and flexibility in the shortfin mako *Isurus oxyrinchus* and the blacktip shark *Carcharhinus limbatus*. *J Morphol* 273(10):1096–1110. <https://doi.org/10.1002/jmor.20047>
- O'Hara KB, Martinez A (2020) Effects of asperity height on monotonic and cyclic interface behavior of bioinspired surfaces under constant normal stiffness conditions. *GeoCongress*. <https://doi.org/10.1061/9780784482834.027>
- O'Hara KB, Martinez A (2020) Monotonic and cyclic frictional anisotropy in snakeskin-inspired surfaces and piles. *J Geotech Geoenv Eng* 146(11):04020116. [https://doi.org/10.1061/\(ASCE\)GT.1943-5606.0002368](https://doi.org/10.1061/(ASCE)GT.1943-5606.0002368)
- Pra-ai S, Boulon M (2017) Soil-structure cyclic direct shear tests: a new interpretation of the direct shear experiment and its application to a series of cyclic tests. *Acta Geotech* 12:107–127. <https://doi.org/10.1007/s11440-016-0456-6>
- Samanta M, Punetha P, Sharma M (2018) Influence of surface texture on sand-steel interface strength response. *Géotechn Lett* 8(1):1–9. <https://doi.org/10.1680/jgele.17.00135>
- Schanz T, Vermeer P (1996) Angles of friction and dilatancy of sand. *Géotechnique* 46(1):145–151
- Stutz HH, Doose R, Wuttke F (2018) Open science interface shear device. In: W Wu, HS Yu (eds) *Proceedings of China-Europe conference on geotechnical engineering*. vol 1, Springer,

- Springer Series in Geomechanics and Geoengineering 1: 615–618, Vienna, Austria, [https://doi.org/10.1007/978-3-319-97112-4\\_137](https://doi.org/10.1007/978-3-319-97112-4_137)
30. Stutz HH, Martinez A, Heepe L, Tramsen HT, Gorb SN (2019) Strength anisotropy at soil-structure interfaces with snake skin inspired structural surfaces. In: Ibraim E, Tarantino A (eds) 7th international symposium on deformation characteristics of geomaterials, IS-Glasgow 2019, 13008, EDP Sciences, E3S Web of Conferences, vol. 92, 7th international symposium on deformation characteristics of geomaterials, Glasgow, United Kingdom. <https://doi.org/10.1051/e3sconf/20199213008>
  31. Subba Rao KS, Allam MM, Robinson RG (1998) Interfacial friction between sands and solid surfaces. Proceedings of the Institution of Civil Engineers Geotech Eng 131(2):75–82. <https://doi.org/10.1680/igeng.1998.30112>
  32. Taylor DW (1948) Fundamentals of soil mechanics. Wiley, New York
  33. Tong Z, Fu P, Zhou S et al (2014) Experimental investigation of shear strength of sands with inherent fabric anisotropy. Acta Geotech 9(April):257–275. <https://doi.org/10.1007/s11440-014-0303-6>
  34. Tramsen HT, Gorb SN, Zhang H, Manoonpong P, Dai Z, Heepe L (2018) Inversion of friction anisotropy in a bio-inspired asymmetrically structured surface. J Royal Soc Interface 15(138):20170629. <https://doi.org/10.1098/rsif.2017.0629>
  35. Uesugi M, Kishida H, Tsubakihara Y (1988) Behavior of sand particles in sand-steel friction. Soils Found 28(1):107–118
  36. Wong RKS, Arthur JRF (1985) Induced and inherent anisotropy in sand. Géotechnique 35(4):471–481
  37. Zhang G, Wang L, Zhang J-M (2011) Dilatancy of the interface between a structure and gravelly soil. Geotechnique 61(1):75–84
  38. Zhang G, Zhang J-M (2006) Monotonic and cyclic tests of interface between structure and gravelly soil. Soils Found 46(4):505–518
- Publisher's Note** Springer Nature remains neutral with regard to jurisdictional claims in published maps and institutional affiliations.